

**Maurício Felga Gobbi**

gobbi@ufpr.br  
Departamento de Engenharia Ambiental  
Universidade Federal do Paraná  
81531-990 Curitiba, PR, Brazil

**Roger Paul Dorweiler**

roger.dorweiler@lactec.org.br  
LACTEC, BR116 km 98 S/N  
Centro Politécnico – UFPR  
Curitiba, PR, Brazil

# Simulation of Wind Over a Relatively Complex Topography: Application to the Askervein Hill

*In this paper we investigate the flow of wind over a relatively complex topography at the lower portion of the atmospheric boundary-layer, by using the well known general purpose CFD package ANSYS-CFX-11. The work was motivated by the difficulty in choosing the optimal locations for turbines (micrositing) in regions of good energy potential, but with complex topography. The simulations were compared with data from landmark experiment at Askervein Hill - Scotland, in 1983. The resulting simulations also were compared favorably with the results of another package for wind simulation.*

**Keywords:** wind turbines, atmospheric boundary-layer, Askervein, CFD

## Introduction

In order to minimize the costs and maximize the efficiency of wind-generated power systems, knowledge about the spatial wind distribution is mandatory for the micrositing – that is, the identification of areas with best possible energy supply. In many developed countries, micrositing is done with the help of very dense meteorological observation networks and some standard models.

In less developed countries, meteorological data can be very scarce, and the application of those models not anchored by a robust observational base is more difficult. Besides, in many regions – for instance in Brazil – even if synoptic wind conditions are known, the overly complex geometry makes micrositing an even more difficult task (Amarante et al. , 2007).

The need to understand the topographic effects on the wind in a small scale leads to several research works, such as Jackson and Hunt (1975) development of a linear theory for the effects of the perturbation caused by mild-sloped hills in two dimensions. This theory was extended to three dimensions by Mason and Sykes (1979).

Standard commercial packages for wind simulation used by the energy industry, like WAsP (Troen and Peterson, 1989) or WindMap (Brower et al. , 2002), are limited to terrains with relatively little complexity. More recently new commercial packages were developed specifically for wind-power applications, these include WindSim (Leroy, 1999) (information at <http://windsim.com/>) and Garrad Hassan (information at <http://www.garradhassan.com/>). These packages can simulate the wind over more complex terrains, including effects of boundary layer separation, and to some extent, effects of atmospheric stability.

Bowen and Mortensen (1996) introduced the Ruggedness Index (RIX), in an attempt to quantify the terrain complexity: it is the percentage of the terrain in a circular area with a 7,000 m diameter, in which the slope exceeds 18°. If RIX exceeds 30%, the terrain is considered complex.

As a general rule, all works indicate that the wind flow over real terrains is quite variable and strongly dependent on the terrain complexity, besides the daily and seasonal variations, and stability/stratification conditions.

In this work we simulate the effects of a complex terrain on the wind flow, using a general purpose CFD package – ANSYS CFX11 (<http://www.ansys.com>). The simulations are done with quite high resolution to minimize grid size dependency. Several closure models for the turbulent sub-grid effects were used and compared amongst each other.

We apply the model to the Askervein Hill – Scotland, where a landmark experiment was held (Taylor and Teunissen, 1983, 1985, 1987), and compare the simulations to both measured data and WindSim model simulations found in Leroy (1999).

More recent works on wind flows over Askervein Hill using CFD include the following. Chow and Street (2009) used Askervein as a framework to show improvements over Large Eddy Simulation (LES) models by the inclusion of a mix of self-similarity and eddy-viscosity in turbulence modeling. Golaz et al. (2009) studied a one-way nested LES system applied to Askervein. Castro et al. (2003) and Stangroom (2004) used a  $\kappa$ - $\epsilon$  model to simulate flow over and around Askervein. As a follow up to Castro et al. (2003), Silva Lopes et al. (2007) modeled the flow at that same location using LES. Memon and KJondreddi (2011) tested four different turbulence closure models for the same problem.

We deliberately did not use Large Eddy Simulation (LES) modeling due to the need for higher horizontal and vertical resolution and high computational costs. For LES simulations and comparisons with other methods, see Silva Lopes et al. (2007) and Chow and Street (2009), among others.

The paper is organized as follows. In the section *Theoretical Background and Model* a short overview of the theory is shown. In *The Askervein Hill Experiment* we overview the experimental data with which we shall compare the simulations. In *Computational Domain and Model Setup* we discuss the domain discretization, and the model setup including boundary conditions. Then in *Comparisons and Results* we show results and compare our simulations amongst themselves, with other models, and with measured data. Finally, in *Conclusions* we discuss the results of the paper.

## Nomenclature

$C_1$	= constant for turbulence closure model
$C_2$	= constant for turbulence closure model
$C_3$	= constant for turbulence closure model
$C_\mu$	= constant for turbulence closure model
$C_\epsilon$	= constant for turbulence closure model
$C_{\epsilon 2}$	= constant for turbulence closure model
$C_{s1}$	= constant for turbulence closure model
$C_{s2}$	= constant for turbulence closure model
$C_{r1}$	= constant for turbulence closure model
$C_{r2}$	= constant for turbulence closure model
$C_{r3}$	= constant for turbulence closure model
$C_{r4}$	= constant for turbulence closure model
$C_{r5}$	= constant for turbulence closure model
$c_s$	= constant for turbulence closure model

Paper received 22 March 2010. Paper accepted 31 October 2011  
Technical Editor: Domingos Alves Rade

$\Delta z_s$	= vertical grid size at the surface
$E_{BB}$	= squared eddy viscosity gradient
$\mathbf{g} \equiv g_i$	= gravitational acceleration
$L_{vk}$	= Von Kármán length scale
$k$	= turbulent kinetic energy
$P, P_{ij}$	= turbulence production
$p$	= pressure
$s_e$	= constant for turbulence closure model
$S$	= speed-up
$U$	= wind speed at location of interest
$U_{RS}$	= incoming wind speed at reference location
$U_i$	= full velocity
$u_i$	= mean velocity
$u'_i$	= velocity fluctuation
$u^*$	= velocity scale
$u_\tau$	= sheer velocity
$x_i$	= Cartesian coordinates
$Y_R$	= surface roughness
$z_0$	= roughness height

### Greek Symbols

$\Delta Y$	= equivalent sand grain roughness
$\delta_{ij}$	= identity tensor
$\varepsilon$	= turbulent kinetic energy dissipation rate
$\phi_{ij}$	= pressure-strain correlation
$\kappa$	= von Kármán constant
$\mu$	= molecular dynamic viscosity
$\nu$	= molecular kinematic viscosity
$\nu_t$	= eddy kinematic viscosity
$\omega$	= turbulence frequency
$\rho$	= air density
$\sigma$	= constant for closure models
$\sigma_k$	= constant for closure models
$\sigma_\varepsilon$	= constant for closure models
$\sigma_\omega$	= constant for closure models
$\tau_{ij}$	= stress tensor
$\tau_w$	= surface sheer stress

### Theoretical Background and Model

CFX is a general purpose CFD package that leans strongly towards engineering applications (especially Mechanical Engineering). Its use for geophysical applications is much less common. The package solves the three-dimensional compressible Reynolds averaged Navier-Stokes equations (RANS), plus mass conservation, energy conservation, and sub-grid equations for turbulence closure. The numerical method used by CFX solves the equations in fairly arbitrary discretized geometries using the Finite-Volume-Method.

#### Averaged Navier-Stokes equations

In this work we will assume that the flow is incompressible with density  $\rho$ , and the Coriolis effect is negligible. The instantaneous velocity field  $U_i$  can be split into the average  $u_i$  and a turbulent fluctuation  $u'_i$  (where Einstein's notation is implied in a Cartesian system  $x_i$ ,  $i = 1, 2, 3$ ):

$$U_i = u_i + u'_i. \quad (1)$$

The same idea applies to the mean pressure field  $p$  and any instantaneous field in the problem. When substituting the above

expression into the nonlinear term of the Navier-Stokes equation a Reynolds stress symmetric tensor appears after averaging:

$$\tau_{ij} = \rho \overline{u'_i u'_j} \quad (2)$$

and needs to be modeled as it involves non-resolved scales. Reynolds stress models solve directly a partial differential equation system involving the six  $\tau_{ij}$  components. Eddy viscosity models work in a similar manner, but the sub-grid and mixing/transport effect of turbulence is accounted for in a viscous-like term.

We assume gravitational acceleration  $\mathbf{g}$  pointing in the  $-x_3$  direction, that is:  $g_i = (0, 0, -g)$ . Mass conservation (incompressible):

$$\frac{\partial u_i}{\partial x_i} = 0. \quad (3)$$

For eddy viscosity models, the momentum reads:

$$\frac{\partial u_i}{\partial t} + u_j \frac{\partial u_i}{\partial x_j} = -\frac{1}{\rho} \frac{\partial p}{\partial x_i} \left( p + \frac{2}{3} \rho k \right) + g_i + \frac{\partial}{\partial x_j} \left[ (\nu + \nu_t) \frac{\partial u_i}{\partial x_j} \right], \quad (4)$$

where  $p$  is the equilibrium thermodynamic pressure field,  $k \equiv \overline{u'_i u'_i}$  is the turbulent kinetic energy,  $\nu$  and  $\nu_t$  are the molecular viscosity and eddy viscosity respectively,  $k$  and  $\nu_t$  are unknowns that should contain all the effects due to the Reynolds stresses. For Reynolds stress models, the momentum equation reads:

$$\frac{\partial u_i}{\partial t} + u_j \frac{\partial u_i}{\partial x_j} = -\frac{1}{\rho} \frac{\partial p}{\partial x_i} + g_i + \frac{\partial}{\partial x_j} \left( \nu \frac{\partial u_i}{\partial x_j} \right) - \frac{\partial (\overline{u'_i u'_j})}{\partial x_j}, \quad (5)$$

where the last term accounts for the Reynolds stresses transport.

#### Turbulence closure models

To determine  $k$  and  $\nu_t$  or  $\overline{u'_i u'_j}$ , a closure model is needed, and in this paper we tested several options available in the CFX package, namely:

1. Zero equation model.
2. One equation  $k - \varepsilon$  eddy viscosity model.
3.  $k - \varepsilon$  model.
4. RNG  $k - \varepsilon$  model.
5.  $k - \omega$  model.
6. Baseline  $k - \omega$  model.
7. SSG Reynolds stress model (Speziale et al. , 1991).
8. Baseline  $\omega$  Reynolds stress model.

Since every closure model has some degree of arbitrariness due to the presence of constants, we have decided not to use those degrees of freedom as calibration parameters, but simply use the literature values that are recommended and set as default by the software developer (ANSYS).

#### Zero equation model

The simplest model of all assumes a constant global value for the eddy viscosity and has very little validity. We added this model here only for the sake of completeness.

**One equation  $k - \varepsilon$  eddy viscosity model**

This model is a simplified version of the traditional  $k - \varepsilon$  model, and was proposed by Menter (1993, 1994, 1997). The kinematic eddy viscosity  $\nu_t$  is modeled by

$$\frac{\partial(\rho \nu_t)}{\partial t} + \frac{\partial(\rho u_i \nu_t)}{\partial x_i} = C_1 \rho \nu_t - C_2 \rho E_{1e} + \left[ \left( \mu + \frac{\rho \nu_t}{\sigma} \right) \frac{\partial(\nu_t)}{\partial x_i} \right], \quad (6)$$

where  $\mu$  is the dynamic viscosity, and

$$E_{1e} = C_3 E_{BB} \tanh \left( \frac{\nu_t}{L_{vk}} \right)^2, \quad (7)$$

$L_{vk}$  is the Von Kármán length scale. As in Menter (1994, 1997),  $C_1 = 0.144$ ,  $C_2 = 1.86$ ,  $C_3 = 7.0$ ,  $\sigma = 1$ , and

$$E_{BB} = \frac{\partial(\nu_t)}{\partial x_i} \frac{\partial(\nu_t)}{\partial x_i}. \quad (8)$$

**$k - \varepsilon$  / RNG  $k - \varepsilon$  model**

The equations for turbulent kinetic energy  $k$  and the dissipation rate  $\varepsilon$  are:

$$\frac{\partial(\rho k)}{\partial t} + \frac{\partial(u_j \rho k)}{\partial x_j} = \frac{\partial}{\partial x_j} \left[ \left( \mu + \frac{\mu_t}{\sigma_k} \right) \frac{\partial k}{\partial x_j} \right] + P - \rho \varepsilon, \quad (9)$$

$$\begin{aligned} \frac{\partial(\rho \varepsilon)}{\partial t} + \frac{\partial(u_j \rho \varepsilon)}{\partial x_j} &= \frac{\partial}{\partial x_j} \left[ \left( \mu + \frac{\mu_t}{\sigma_\varepsilon} \right) \frac{\partial \varepsilon}{\partial x_j} \right] \\ &+ \frac{\varepsilon}{k} (C_{\varepsilon 1} P - C_{\varepsilon 2} \rho \varepsilon), \end{aligned} \quad (10)$$

The turbulent kinetic energy  $k$ , the dissipation rate  $\varepsilon$ , and the eddy viscosity  $\nu_t$  are related by:

$$\nu_t = C_\mu \frac{k^2}{\varepsilon}. \quad (11)$$

$P$  is a production term which, neglecting buoyancy and assuming incompressibility, is calculated by:

$$P = \mu_t \frac{\partial u_i}{\partial x_j} \left( \frac{\partial u_j}{\partial x_i} + \frac{\partial u_i}{\partial x_j} \right). \quad (12)$$

The  $k - \varepsilon$  (RNG- $k - \varepsilon$ ) model's non-dimensional parameters used in this work are fixed constants in CFX and are given by:

$$\begin{aligned} C_\mu &= 0.09(0.085), \quad C_{\varepsilon 1} = 1.44(1.42), \quad C_{\varepsilon 2} = 1.92(1.68), \\ \sigma_k &= 1.0, \quad \sigma_\varepsilon = 1.3, \end{aligned} \quad (13)$$

while the RNG analysis suggests that the otherwise constant parameter  $C_{\varepsilon 1}$  be calculated as the function:

$$\begin{aligned} C_{\varepsilon 1} &= 1.42 - \frac{\eta - (1 - \frac{\eta}{4.38})}{1 + 0.012\eta^3}, \\ \eta &= \sqrt{\frac{\nu_t}{C_\mu \varepsilon} \frac{\partial u_i}{\partial x_j} \left( \frac{\partial u_i}{\partial x_j} + \frac{\partial u_j}{\partial x_i} \right)}. \end{aligned} \quad (14)$$

**$k - \omega$  model**

The  $k - \omega$  model we used was proposed by Wilcox (1986) and others. We neglected buoyancy forcing terms. The model is somewhat similar to the  $k - \varepsilon$  model but solves the turbulent frequency variable  $\omega \equiv \varepsilon/k$ . The model is suitable for lower Reynolds number computations near solid boundaries, and is very sensitive to open boundaries. We do not expect a good performance for the kind of problem we are dealing in this paper. Nevertheless, the model is included for the sake of completeness. The equations are:

$$\frac{\partial(\rho k)}{\partial t} + \frac{\partial(u_j \rho k)}{\partial x_j} = \frac{\partial}{\partial x_j} \left[ \left( \mu + \frac{\mu_t}{\sigma_k} \right) \frac{\partial k}{\partial x_j} \right] + P - \beta' \rho k \omega, \quad (15)$$

$$\begin{aligned} \frac{\partial(\rho \omega)}{\partial t} + \frac{\partial(u_j \rho \omega)}{\partial x_j} &= \frac{\partial}{\partial x_j} \left[ \left( \mu + \frac{\mu_t}{\sigma_\omega} \right) \frac{\partial \omega}{\partial x_j} \right] \\ &+ \frac{\alpha \omega}{k} P - \beta \rho \omega^2, \end{aligned} \quad (16)$$

where  $P$  is calculated as in Eq. (12),  $\beta' = 0.09$ ,  $\alpha = 5/9$ ,  $\beta = 0.075$ ,  $\sigma_k = \sigma_\omega = 2$ .

**Baseline  $k - \omega$  model**

The Baseline  $k - \omega$  model combines the  $k - \omega$  model near the surface with a  $k - \varepsilon$  (transformed to  $k - \omega$ ) model at the “free-stream” portion of the domain (Menter, 1993). This model fixes the open boundary problem mentioned above. The two models are blended together by a blending function. The reader is referred to Menter (1994) for details.

**SSG-Reynolds stress**

Reynolds stress models will predict all components of the covariances of the velocity fluctuations, the equations for the stresses transport and the dissipation rate:

$$\begin{aligned} \frac{\partial(\rho \overline{u'_i u'_j})}{\partial t} + \frac{\partial(u_k \rho \overline{u'_i u'_j})}{\partial x_k} &= \frac{\partial}{\partial x_k} \left[ \left( \mu \delta_{kl} + \frac{c_s \rho k \overline{u'_k u'_l}}{\varepsilon} \right) \frac{\partial(\overline{u'_i u'_j})}{\partial x_l} \right] \\ &- \frac{2\delta_{ij} \rho \varepsilon}{3} + P_{ij} + \phi_{ij}, \end{aligned} \quad (17)$$

$$\begin{aligned} \frac{\partial(\rho \varepsilon)}{\partial t} + \frac{\partial(u_j \rho \varepsilon)}{\partial x_j} &= \frac{\partial}{\partial x_j} \left[ \left( \mu + \frac{\mu_t}{\sigma_\varepsilon} \right) \frac{\partial \varepsilon}{\partial x_j} \right] \\ &+ \frac{\varepsilon}{k} (C_{\varepsilon 1} P - C_{\varepsilon 2} \rho \varepsilon) \\ &+ \frac{\partial}{\partial x_k} \left[ \left( \mu \delta_{kl} + \frac{c_s \rho k \overline{u'_k u'_l}}{\varepsilon} \right) \frac{\partial(\varepsilon)}{\partial x_l} \right], \end{aligned} \quad (18)$$

where the production tensor

$$P_{ij} = \left( \overline{u'_i u'_j} \right) \left( \frac{\partial u_i}{\partial x_k} + \frac{\partial u_k}{\partial x_i} \right). \quad (19)$$

The pressure-strain correlation  $\phi_{ij}$  is given by:

$$\begin{aligned} \phi_{ij} = & -\rho\varepsilon \left[ C_{s1}a_{ij} + C_{s2} \left( a_{ik}a_{kj} - \frac{a_{kl}a_{kl}\delta_{ij}}{3} \right) \right] \\ & - C_{r1}Pa_{ij} + C_{r2}\rho k S_{ij} - C_{r3}\rho k S_{ij} \sqrt{a_{kl}akl} \\ & + C_{r4}\rho k \left( a_{ik}S_{kj} + S_{jk}a_{ki} - \frac{2a_{kl}S_{kl}\delta_{ij}}{3} \right) \\ & + C_{r4}\rho k (a_{ik}W_{kj} + W_{jk}a_{ki}), \end{aligned} \quad (20)$$

where

$$\begin{aligned} a_{ij} &= \frac{\overline{u_i' u_j'}}{k} - \frac{2\delta_{ij}}{3}, \quad S_{ij} = \frac{1}{2} \left( \frac{\partial u_i}{\partial x_j} + \frac{\partial u_j}{\partial x_i} \right), \\ W_{ij} &= \frac{1}{2} \left( \frac{\partial u_i}{\partial x_j} - \frac{\partial u_j}{\partial x_i} \right). \end{aligned} \quad (21)$$

The constants used in the present paper were (Speziale et al., 1991):  $C_\mu = 0.1$ ,  $s_e = 1.36$ ,  $c_s = 0.22$ ,  $C_{\varepsilon 1} = 1.45$ ,  $C_{\varepsilon 2} = 1.83$ ,  $C_{s1} = 1.7$ ,  $C_{s2} = -1.05$ ,  $C_{r1} = 0.9$ ,  $C_{r2} = 0.8$ ,  $C_{r3} = 0.65$ ,  $C_{r4} = 0.625$ ,  $C_{r5} = 0.2$ .

### Baseline $\omega$ Reynolds stress model

In a similar fashion to the  $k-\varepsilon$  and  $k-\omega$  models described above, a Reynolds stress model can be derived with the turbulent frequency  $\omega$  in place of an equation for the dissipation  $\varepsilon$ . This model has the same advantages and limitations as the  $k-\omega$  model, and, analogously to the previous models, a blending can be done in which, far from the solid boundaries (surface), one can use the  $\varepsilon$  equation in place of the  $\omega$  equation, to avoid the extreme sensitivity to the unknown conditions at the domain's open boundaries. The resulting model is what we call Baseline  $\omega$  Reynolds stress model.

### Surface layer and bottom boundary condition

The surface boundary conditions used in the present paper are based on the classic logarithmic profile (see below) of the surface layer developed by Launder and Spalding (1974). Because this application involves reasonably large scales, the grid spacing at the surface will be much larger than the viscous layer, and the no-slip condition needs to be substituted by some sort of near-wall formulation/parameterization. The average velocity at the boundary is assumed to be far enough from the viscous layer, and is linked to the shear stress through a logarithmic function (*wall-law*).

The wall (surface) shear stress is given by:

$$\tau_w = \rho u^* u^\tau, \quad (22)$$

where

$$u^\tau = u \left[ \frac{1}{\kappa} \ln \left( \frac{y^*}{1 + 0.3Y_R u^*/\nu} \right) + 5.2 \right]^{-1}, \quad (23)$$

$$y^* = \frac{u^* \Delta Y}{\nu}, \quad (24)$$

and where  $\kappa = 0.41$  is the usual von Kármán constant,  $Y_R$  is a measurement of the surface roughness,  $\Delta Y$  (*equivalent sand grain roughness*) is the vertical distance at which we have the actual modeled surface velocity  $u$ .

### The Askervein Hill Experiment

The Askervein Hill project (Taylor and Teunissen, 1983, 1985, 1987) was a cooperative effort to study the flow in the low part of the

atmospheric boundary layer and how it was affected by the presence of a hill. The project was sponsored by the *International Energy Agency Research and Development Wind Energy Conversion Systems*. This study consisted in the installation of over 50 wind measurement stations (where cup, Gill UVW, and sonic anemometers were used) which operated for two 16-day periods in September/October of 1982 and 1983. The measurements took place over and around the Askervein Hill on the west coast of the South Uist island – Outer Hebrides – Scotland ( $57^\circ 11' N$ ,  $7^\circ 22' W$ ). Besides the wind measurements at the fixed stations, there were also several measurements of the weather conditions such as: TALA – Tethered Aerodynamic Lifting Anemometer – or *Kite Systems*, which give the wind profile up to 200 m height; and AIRsonde to give the atmospheric profile up to 2,000 m heights.

The main goal of the project was to know in great detail the wind field (mean and turbulent fluctuations) just above the ground (around 10 m) on a typical region for the installation of a wind power farm. The resulting data have become of great value for model calibration purposes. The hill has an approximately elliptic shape with axes of 2 km and 1 km, and a maximum height of 116 m above its base and 126 m above sea level. Fig. 1 shows an aerial view and the distribution of the measurement towers/posts at cross sections A-A, AA-AA, B-B. Most towers were 10 m high, but there were also towers/posts of heights 17 m, 30 m, and 50 m, and some of them measured wind at several heights. The figure also shows the locations of the stations on the top/center of the hill, HT (highest point) and CP (center point). There is also a 50 m high reference station RS (not shown in the illustration), where the reference wind is unaffected by the presence of the hill. The directions A-A and AA-AA, are aligned with the average measured wind, and also with the model's incident wind direction.

For the sake of shortness we will not present here the resulting measurements. Some results will be presented in summarized form in a later section. For details the reader is referred to the project's original reports.

### Computational Domain and Model Setup

A computational domain was defined on the region shown in Fig. 1.

The terrain information for the present work was obtained from the Askervein Hill project as a file covering an area of  $6,000 \text{ m} \times 6,000 \text{ m}$ , with each point representing a projected horizontal square cell with area  $23.4375 \text{ m} \times 23.4375 \text{ m}$ .

Modeling the terrain properly and then exporting it to match the choice of finite volumes at the bottom boundary of the domain is a quite laborious task and should not be underestimated.

Several tests were done to check grid refinement impact, starting with average horizontal size of the elements at approximately 23 m (compatible with terrain resolution) and over 5 million volumes. Grid size was then progressively increased until the differences in the results were no longer negligible. The final choice was to discretize the domain with average horizontal size of approximately 40 m, and 1,200,000 (1.2 million) elements were necessary to cover the entire domain. We used tetrahedron unstructured finite volumes starting 15 m above the ground and up to 1,000 m (top boundary), where we assume that the surface has little effect on the flow, given that the stability condition is neutral. The bottom faces of those elements define the horizontal reach of the computational domain and can be seen in Fig. 2-top. Notice the finer discretization on the top of the hill. From the surface (ground) to the bottom of the unstructured grid, a prismatic structured grid was used to refine the region inside the first



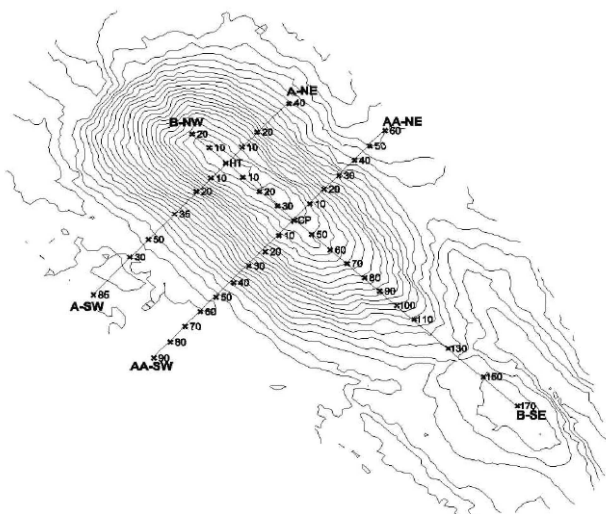
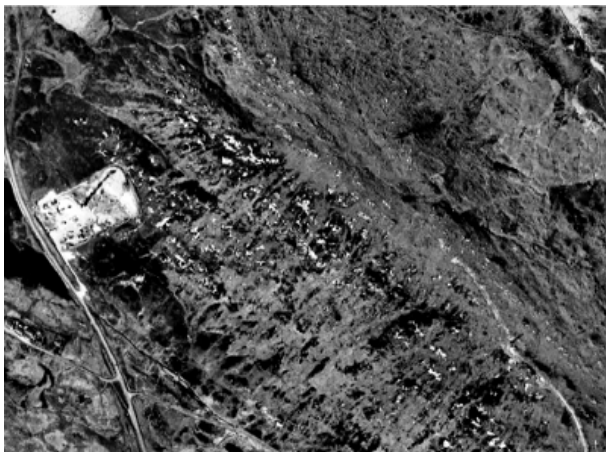


Figure 1. Askervein Hill project: aerial view and measurement stations.

15 m above the ground, and the structured and the unstructured grids were forced to match at 15 m height. Within this 15 m region, five different structured sub-meshes with grid height  $\Delta z_s$  were used and merged with the above unstructured grid, namely: (i) 3 layers with  $\Delta z_s = 5$  m; (ii) 5 layers with  $\Delta z_s = 3$  m; (iii) 10 layers with  $\Delta z_s = 1.5$  m; (iv) 15 layers with  $\Delta z_s = 1$  m; (v) 30 layers with  $\Delta z_s = 0.5$  m.

Fig. 2-bottom shows a 3-D view of the bottom of the domain where the near-surface discretization can be seen.

**Boundary and initial conditions**

**Bottom boundary**

ANSYS CFX requires boundary conditions at all boundaries. We have already discussed the surface (bottom) boundary conditions used in this paper, remaining only to mention that, following the Askervein project reports, we used the surface roughness height value  $z_0 = 0.03$  m. Also, the parameter  $Y_R$  used in this work was not the one suggested by the CFX manual  $Y_R = 30z_0$ , but  $Y_R = 7.5z_0$ , suggested by Brutsaert (1982), which is more appropriate for natural surfaces.

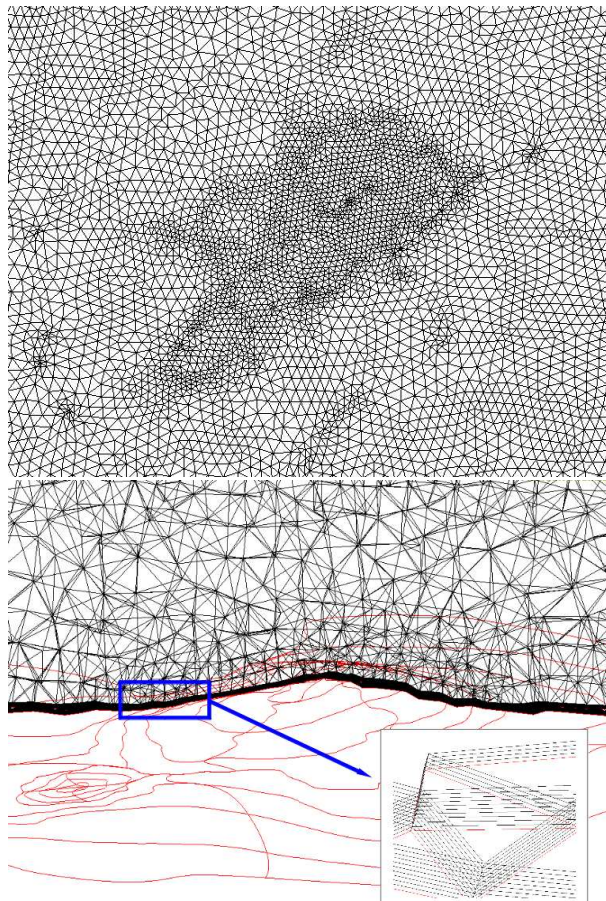


Figure 2. Discretized domain at the surface – horizontal view (top) and 3-D view (bottom).

**Lateral and top boundaries**

At the sides (lateral) and top boundaries, a zero-normal velocity condition was used (free-slip). Since these lateral boundaries are relatively far from the region of interest (center of the domain) the wall boundary condition did not seem to affect the solution. At the exit (behind the hill), a free outflow radiation condition was used. The pressure distribution used was hydrostatic, based on the local temperature and pressure conditions during the experiments.

**Inflow boundary**

For the inlet condition, where a Reynolds averaged velocity profile and the sub-grid turbulent kinetic energy and dissipation rate must be specified, we used the *zero-gradient* condition for the sub-grid turbulence variables. Several combinations of vertical profiles for different stretches of the atmospheric boundary layer were tested for the velocity at the inlet and we have found that the best one was to use a classic log profile, making sure that the velocity matched as well as possible the measurements at the reference tower, AIRsonde, and the synoptic condition during the experiments. The profile is shown in Fig. 3

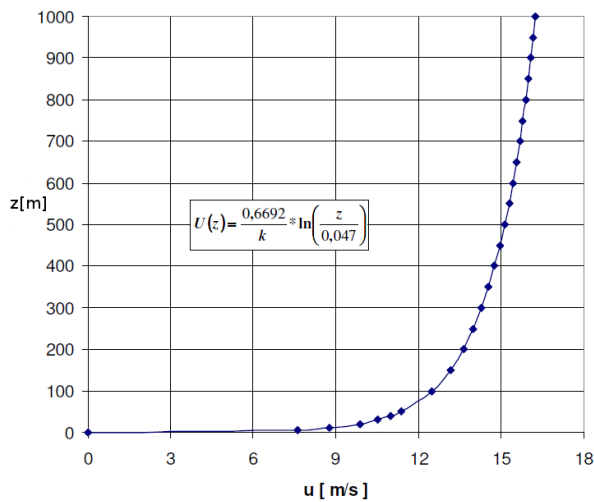


Figure 3. Profile for the inflow boundary condition.

**Initial condition**

In the present work only stationary results were sought and initial conditions only change the number of iterations before each run reaches the steady state. The condition used for this purpose was the inflow condition for the entire domain.

**Comparisons and Results**

We present the resulting simulations in terms of the speed-up  $S$ , defined as:

$$S = \frac{U - U_{RS}}{U_{RS}}, \tag{25}$$

where  $U$  is the simulated wind speed 10 m above the surface, and  $U_{RS}$  is the wind modeled at the reference station (inlet boundary condition). All simulations are compared with the measurements (with error bar) exactly as provided by the Askervein experiments.

Fig. 4 shows, for sections A-A, AA-AA, and B-B, comparisons between Askervein data and the zero-equation model for five different near-surface discretization, as described earlier. It can be seen that this model not only did not perform well with CFX default parameter estimation (all parameters of this model are global), but was insensitive to the grid refinement. We simply disregard this simulation for this model's lack of physical validity.

Fig. 5 shows the results for the one-equation eddy viscosity model. Despite its relative simplicity, this model performs reasonably well over the entire range of measured points. It is a curious fact that the most all around accurate model is not necessarily the one with the most refined vertical grid size at the surface layer. We attribute this to the fact that in many cases the most refined runs showed poorer numerical convergence, probably due to the abrupt change in resolution at the structured-unstructured grid interface. Notice also that in these simulations, the sensitivity of the grid refinement varies a great deal spatially, and as a general rule, the model is less sensitive at higher locations/higher wind speeds.

Fig. 6 shows similar results but now using the two-equation  $k - \epsilon$  model. The  $k - \epsilon$  is one of the most widely used closure models for turbulent flows with large Reynolds Number for its good overall results, particularly for geophysical flows. The present simulation

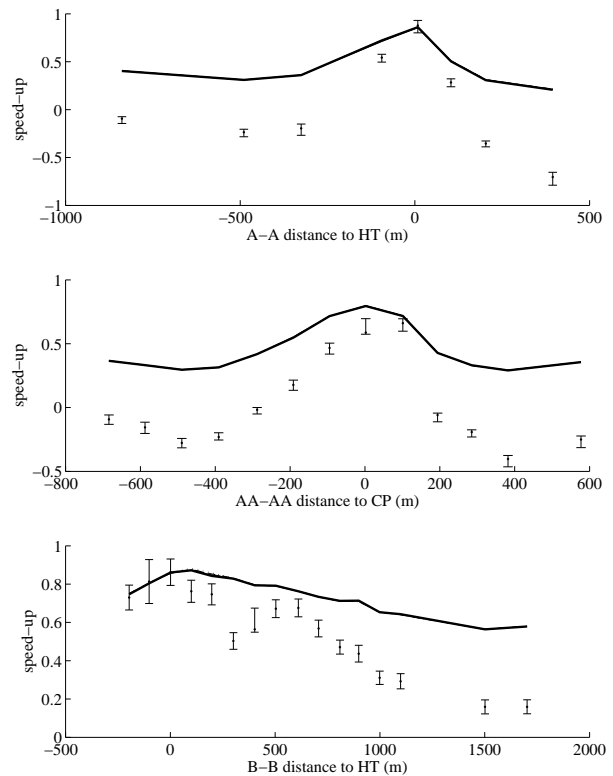


Figure 4. Zero-equation model. Speed-up at sections A-A, AA-AA, and B-B. Near-surface  $\Delta z_s$ : 0.5 m (thick full line), 1.0 m (thin full line), 1.5 m (dot-dashed), 3.0 m (dashed), 5.0 m (dotted).

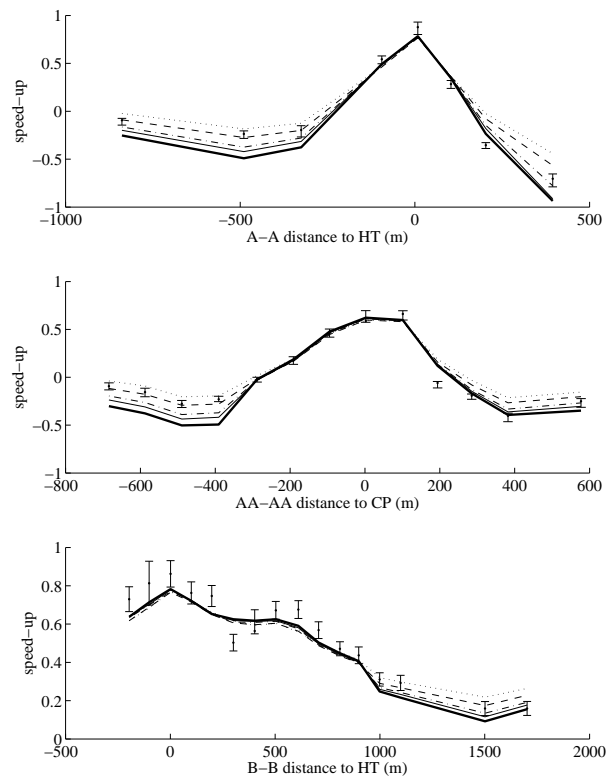


Figure 5. One-equation model. Speed-up at sections A-A, AA-AA, and B-B. Near-surface  $\Delta z_s$ : 0.5 m (thick full line), 1.0 m (thin full line), 1.5 m (dot-dashed), 3.0 m (dashed), 5.0 m (dotted).

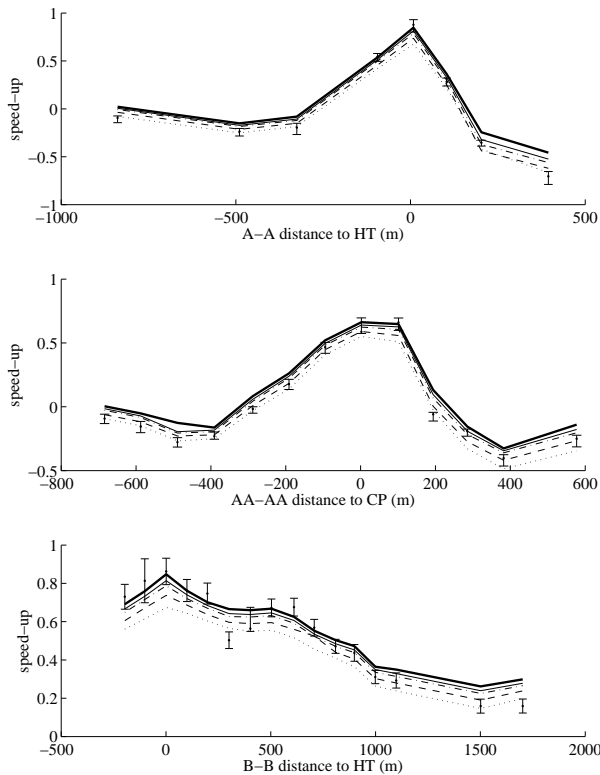


Figure 6.  $k-\varepsilon$  model. Speed-up at sections A-A, AA-AA, and B-B. Near-surface  $\Delta z_s$ : 0.5 m (thick full line), 1.0 m (thin full line), 1.5 m (dot-dashed), 3.0 m (dashed), 5.0 m (dotted).

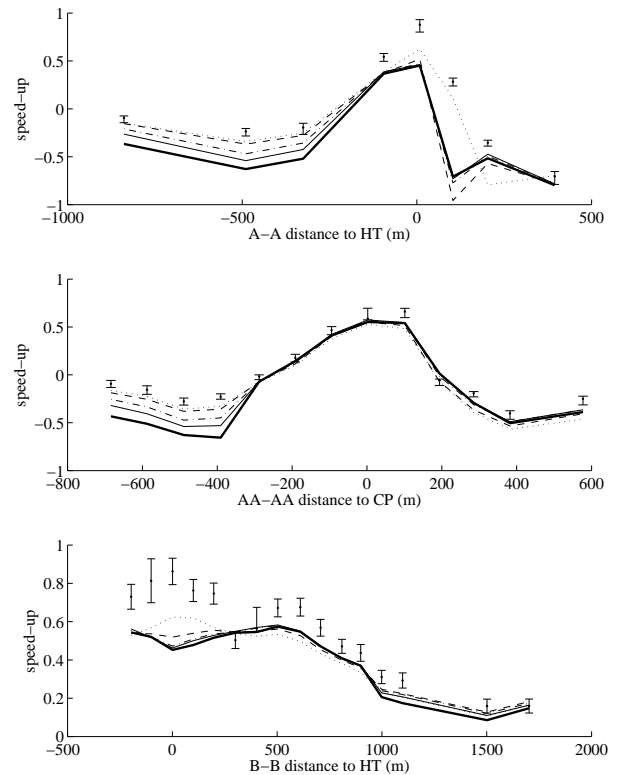


Figure 7. RNG  $k-\varepsilon$  model. Speed-up at sections A-A, AA-AA, and B-B. Near-surface  $\Delta z_s$ : 0.5 m (thick full line), 1.0 m (thin full line), 1.5 m (dot-dashed), 3.0 m (dashed), 5.0 m (dotted).

is no exception, showing that the agreement with data is quite satisfactory. In this case, the changes in the flow field close to the boundary due to grid refinement were much more smooth and uniform than for the one-equation model shown previously, which is an indication that an extra equation for a turbulence parameter to be solved numerically and locally (rather than being set as a constant global parameter) paid off.

The flow behind the Askervein Hill (hill's lee) can separate, and this has been reported as what happened in certain wind conditions. Although the  $k-\varepsilon$  model performs reasonably well, we have also run the so called renormalization group analysis, or the RNG  $k-\varepsilon$  model. This model was developed to better handle separated flows such as flows around abrupt boundary curves. The results are shown in Fig. 7. Although the model clearly shows itself as very sensitive behind the hill and able to drastically drop in the near-ground velocity field in those separation-prone regions, the model also has poorer prediction of the velocity field elsewhere, usually under-predicting the velocity. Even at the separation region, the model showed excessive sensitivity to grid spacing, and, although no parameter sensitivity tests were performed, we conjecture that this is a difficult model to calibrate.

Fig. 8 shows the results for the  $k-\omega$  model. The model performance is quite poor, and that is expected, as this model was designed for surface sub-layers with low Reynolds Number, and this type of flow regime is not resolved in the present case. Added to this, it is well known that the  $k-\omega$  model is extremely sensitive to open Boundary conditions for the two turbulence parameters, and requires extremely accurate values of those at the domain entrances, something rarely known (in the present simulations we used zero gradient for all the scalar variables at the open boundaries).

We also used the so called  $k-\omega$  Baseline model, which combines a  $k-\omega$  model in the vicinity of solid boundaries (the surface in the present case) with a  $k-\varepsilon$  model elsewhere. As can be seen in Fig. 9, the results were, expectedly, much better than the ones with the  $k-\omega$  model alone, and the convergence rate as the grid was refined, was the most robust of all models tested here. The accuracy, compared to data, was overall worse than for the  $k-\varepsilon$  model, and much worse at the hill's lee. Again, even for the lower portion of the domain, the present problem has too high Reynolds Numbers to justify the use of a  $k-\omega$  formulation, but we thought it would be an interesting test to see how the model would perform.

Fig. 10 shows results for what we called SSG Reynolds Stress model. This is a closure scheme that solves all six Reynolds Stress components, and the constants of the model are given by Speziale et al. (1991). The results were poorer than we expected. Similarly to what happens with  $k-\varepsilon$  models, one of the problems with the Reynolds Stress models is its poor capability of resolving near-wall (low Reynolds Number) stresses. To overcome this problem several mixed models have been proposed, amongst which the one shown here, which we call Baseline Reynolds Stress model. This model blends with a  $k-\omega$  Baseline model near solid surfaces, as an attempt to overcome its weakness. The results of this model applied to our problem are shown in Fig. 11. The model performed reasonably well, except at the hill's lee, once again.

Finally, we took some of the best results (compared to data) of the models above and plotted them amongst themselves, against data, and against the best results found in Leroy (1999) using the software WindSim. Those results are shown in Fig. 12 and the present model with  $k-\varepsilon$  closure appeared to outperform the others.

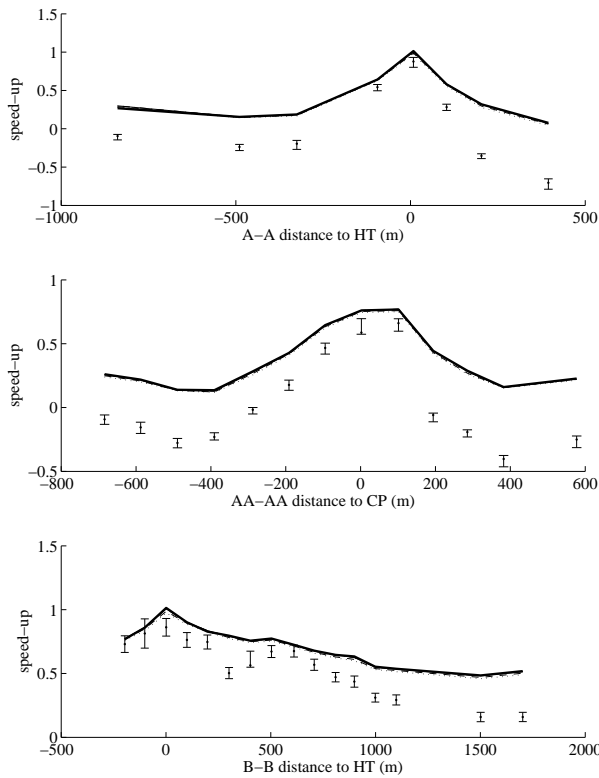


Figure 8.  $k-\omega$  model. Speed-up at sections A-A, AA-AA, and B-B. Near-surface  $\Delta z_s$ : 0.5 m (thick full line), 1.0 m (thin full line), 1.5 m (dot-dashed), 3.0 m (dashed), 5.0 m (dotted).

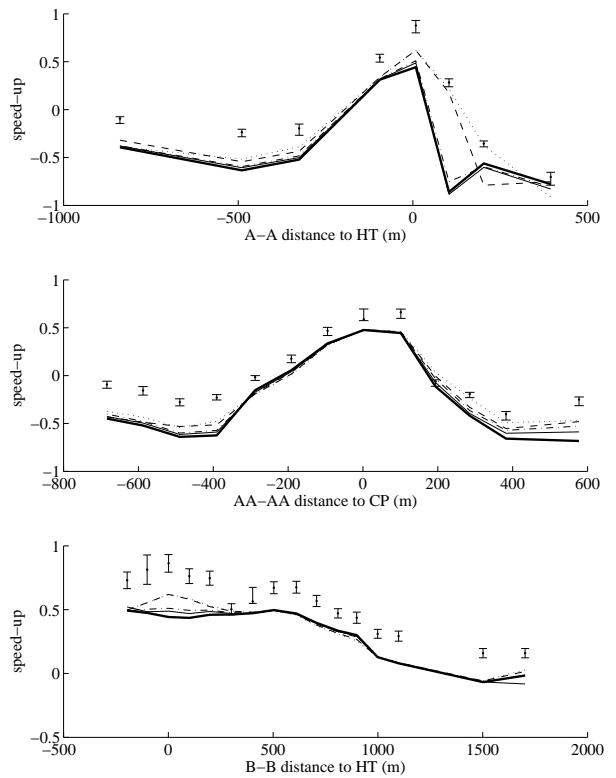


Figure 10. SSG Reynolds stress model. Speed-up at sections A-A, AA-AA, and B-B. Near-surface  $\Delta z_s$ : 0.5 m (thick full line), 1.0 m (thin full line), 1.5 m (dot-dashed), 3.0 m (dashed), 5.0 m (dotted).

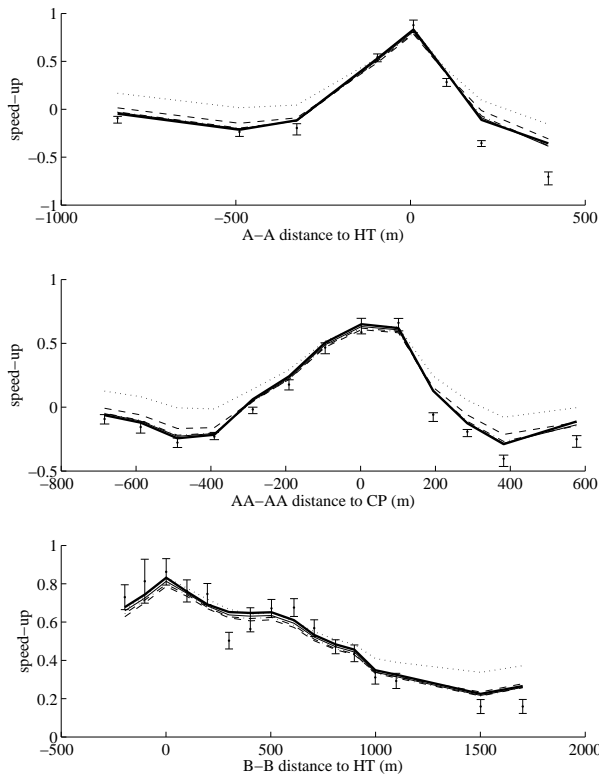


Figure 9.  $k-\omega$  Baseline model. Speed-up at sections A-A, AA-AA, and B-B. Near-surface  $\Delta z_s$ : 0.5 m (thick full line), 1.0 m (thin full line), 1.5 m (dot-dashed), 3.0 m (dashed), 5.0 m (dotted).

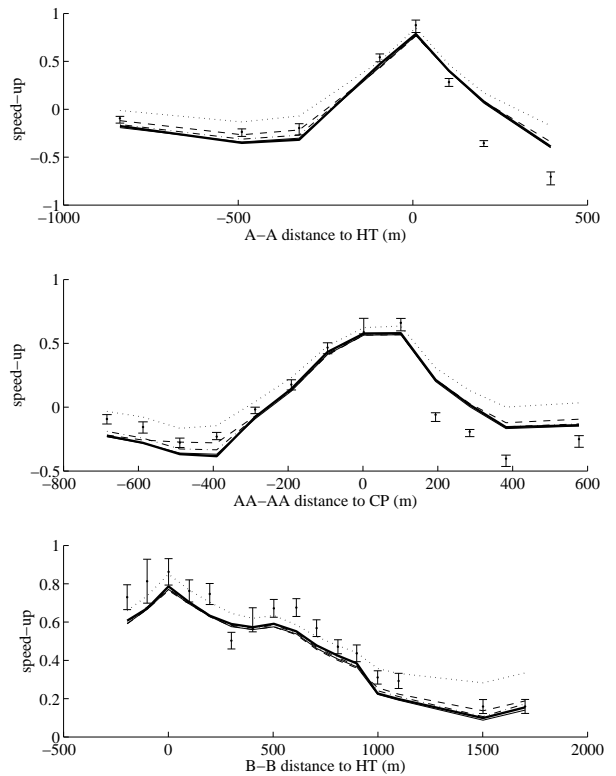


Figure 11. Baseline Reynolds stress model. Speed-up at sections A-A, AA-AA, and B-B. Near-surface  $\Delta z_s$ : 0.5 m (thick full line), 1.0 m (thin full line), 1.5 m (dot-dashed), 3.0 m (dashed), 5.0 m (dotted).



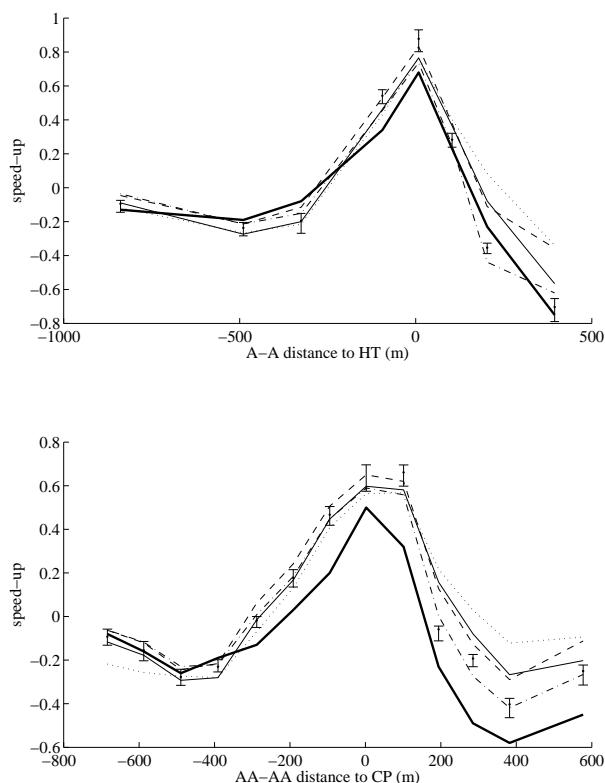


Figure 12. Comparison between models. Speed-up at sections A-A and AA-AA. WindSim (thick full line), CFX one equation model (thin full line), CFX  $k-\epsilon$  model (dot-dashed), CFX  $k-\omega$  Baseline model (dashed), Baseline Reynolds stress model (dotted).

## Conclusions

This paper was motivated by the need for a tool to help understanding wind over complex terrains for micro-siting of wind energy plants.

Several closure methods were tested in CFX's turbulence module when applied to the problem of wind over the Askervein Hill, for which there are extensive data available.

The authors chose not to use Large Eddy Simulations due to its computational costs.

The results showed that the  $k-\epsilon$  model had the best overall performance, with reasonably robust and smooth behavior and convergence rate as the grid size is reduced near the ground.

Finally, it is clear that the use of CFX as a tool for wind power plant micro-siting is quite possible for flows over relatively complex terrain. More field experimental data sets are needed to confirm the present conclusions.

## Acknowledgements

We would like to express our gratitude to LACTEC for providing support for this paper.

## References

Amarante, O.A.C. do, Silva F.J.L., Parecy, E., Procopiak L.A.J., Dorweiler, R.P., Schultz, D.J., Souza, M.L. and Anunciao, S.M., 2007. "Wind Energy Resource Map of the State of Paran", Brazil, P&D ANEEL Report – COPEL, Brazil.

Bowen, A. J., Mortensen, N.G., 1996, "Exploring the limits of WAsP the wind atlas analysis and application program", In: Proceedings of European Union Wind Energy Conference, Goteburg, Sweden, pp. 584-587.

Brower, M., Bailey, B. and Zack, J., 2002, "Micro-siting using the MesoMap System", Presented at Winpower 2002 Conference. Portland, Oregon.

Brutsaert, W.H., 1982, "Evaporation into the atmosphere", D. Reidel, Norwell, Mass.

Castro, F.A., Palma, J.M.L.M.B. and Silva Lopes, A., 2003, "Simulation of the Askervein flow. Part 1: Reynolds averaged NavierStokes equations  $k-\epsilon$  turbulence model", *Boundary-Layer Meteorology*, 107, pp. 501-530.

Castro, F.A., Palma, J.M.L.M.B. and Silva Lopes, A., 2009, "Evaluation of Turbulence Closure Models for Large-Eddy Simulation over Complex Terrain: Flow over Askervein Hill", *Journal of Applied Meteorology and Climatology*, Vol. 48, pp. 1050-1065.

Golaz, J.-C., Doyle, J.D. and Wang, S., 2009, "One-Way Nested Large-Eddy Simulation over the Askervein Hill", *J. Adv. Model. Earth Syst.*, Vol. 1, No. 6, pp. 16.

Jackson, P.S. and Hunt, J.C.R., 1975, "Turbulent Wind flow over a low hill", *Quarterly Journal of the Royal Meteorological Society*, Vol. 101, pp. 929-955.

Launder, B.E. and Spalding, D.B., 1974, "The numerical computation of turbulent flows", *Computer Methods in Applied Mechanics and Engineering*, 3(2), pp. 269-289.

Leroy, J., 1999, "Wind field simulations at Askervein hill Internal Report VECTOR AS", Technical Report vector-9910-100, 37 p.

Mason, P.J. and Sykes, R., 1979, "Flow over an isolated hill of moderate slope", *Quart. J. Roy. Meteorol. Soc.*, 105, pp. 383-395.

Menter, F.R., 1994, "Multiscale Models for Tubulent Flows.", 24th Fluid Dynamics Conference, American Institute of Aeronautics and Astronautics.

Menter, F.R., 1994, "Eddy Viscosity Transport Equations and their Relation to the  $k-\epsilon$  Model", NASA Technical Memorandum 108854.

Menter, F.R., 1997, "Eddy Viscosity Transport Equations and their Relation to the  $k-\epsilon$  Model", *ASME J. Fluids Engineering*, Vol. 119, pp. 876-884.

Silva Lopes, A., Castro, F.A. and Palma, J.M.L.M.B., 2007, "Simulation of the Askervein flow. Part 2: Large eddy simulations", *Boundary-Layer Meteorol.*, 125, pp. 851-884.

Speziale, C.G., Sarkar, S. and Gatski, T.B., 1991, "Modelling the pressure-strain correlation of turbulence: an invariant dynamical systems approach", *J. Fluid Mechanics*, Vol. 277, pp. 245-272.

Stangroom, P., 2011, "Wind Resource Assessment in Complex Terrain Using CFD", M.Sc. Thesis - Technical University of Denmark.

Stangroom, P., 2004, "Stangroom", Ph.D. Thesis - University of Nottingham.

Taylor, P.A. and Teunissen, H.W., 1983, "Askervein 82: Report on the September/October 1982 experiment to study boundary-layer flow over Askervein, South Uist", Ontario, Canada, Meteorological Services Research Branch.

Taylor, P.A., Teunissen, H.W., 1985, "The Askervein Hill Project: Report on the September/October 1983, main field experiment", Ontario, Canada, Meteorological Services Research Branch.

Taylor, P.A., Teunissen, H.W., 1987, "The Askervein Hill Project: Overview and background data.", *Boundary Layer Meteorology*, Vol. 39, pp. 15-39.

Troen, I., Peterson, E.L., 1989, European Wind Atlas. National Laboratory, Rskilde, Denmark, ISBN 87-550-1482-8, 656 p.

Wilcox, D.C., 1986, "Multiscale model for turbulent flows", In AIAA 24th Aerospace Sciences Meeting. American Institute of Aeronautics and Astronautics.